Coastal Engineering 57 (2010) 668–683

Contents lists available at ScienceDirect

Coastal Engineering

journal homepage: www.elsevier.com/locate/coastaleng

Two-dimensional time dependent hurricane overwash and erosion modeling at Santa Rosa Island

R.T. McCall [a,b,*], J.S.M. Van Thiel de Vries [a,b], N.G. Plant [c], A.R. Van Dongeren [a], J.A. Roelvink [a,b,d], D.M. Thompson [c], A.J.H.M. Reniers [b,e]

[a] Deltares (formerly Delft Hydraulics), Delft, The Netherlands
[b] Department of Civil Engineering and Geosciences, Delft University of Technology, Delft, The Netherlands
[c] Center for Coastal & Watershed Studies, USGS, St. Petersburg, Florida, USA
[d] Unesco-IHE Institute for Water Education, Delft, The Netherlands
[e] Rosenstiel School of Marine and Atmospheric Science, University of Miami, Florida, USA

ARTICLE INFO

Article history:
Received 20 May 2009
Received in revised form 12 February 2010
Accepted 15 February 2010
Available online 29 March 2010

Keywords:
Overwash
Hurricane impact
XBeach
Dune erosion
Numerical modeling
Morphodynamics
Infragravity waves

ABSTRACT

A 2DH numerical, model which is capable of computing nearshore circulation and morphodynamics, including dune erosion, breaching and overwash, is used to simulate overwash caused by Hurricane Ivan (2004) on a barrier island. The model is forced using parametric wave and surge time series based on field data and large-scale numerical model results. The model predicted beach face and dune erosion reasonably well as well as the development of washover fans. Furthermore, the model demonstrated considerable quantitative skill (upwards of 66% of variance explained, maximum bias −0.21 m) in hindcasting the post-storm shape and elevation of the subaerial barrier island when a sheet flow sediment transport limiter was applied. The prediction skill ranged between 0.66 and 0.77 in a series of sensitivity tests in which several hydraulic forcing parameters were varied. The sensitivity studies showed that the variations in the incident wave height and wave period affected the entire simulated island morphology while variations in the surge level gradient between the ocean and back barrier bay affected the amount of deposition on the back barrier and in the back barrier bay. The model sensitivity to the sheet flow sediment transport limiter, which served as a proxy for unknown factors controlling the resistance to erosion, was significantly greater than the sensitivity to the hydraulic forcing parameters. If no limiter was applied the simulated morphological response of the barrier island was an order of magnitude greater than the measured morphological response.

1. Introduction

The need for predicting the response of coasts to storms is rising steadily as the population in coastal areas grows worldwide and loads on coastal systems increase due to rising sea levels and the possibility of more intense storms (Emanuel et al., 2008). Approximately 10% of the world's coastline consists of barrier coasts (Cromwell, 1971), which are susceptible to beach and dune erosion and coastal flooding. For most barrier coasts, overwash constitutes a natural response to increased hydraulic forcing by storm surge and waves. Overwash is defined as the flow of water and sediment across the crest of a beach or dune that does not directly return to the waterbody where it originated (Donnelly et al., 2004). A distinction is made between runup overwash, which takes place when the runup of individual waves exceeds the beach or dune crest, and inundation overwash, which occurs if the combined storm surge level and wave setup exceeds the crest height (Donnelly et al., 2004; Sallenger, 2000). Sediment that is deposited by overwash is called washover. Washover contributes to the sediment budget of barrier islands and is thought to help maintain the width of barrier islands as they migrate landwards (e.g. Godfrey and Godfrey, 1973; Hosier and Cleary, 1977). Further information about overwash is given in a comprehensive review by Donnelly et al. (2006).

In order to manage overwash in areas where it is not desirable, or to reduce the consequences of overwash, a reliable predictive model is required to assess weak stretches of coast and coastal defense designs. Although of obvious use to coastal managers, the capability to quantitatively predict and simulate overwash and washover volumes is only just beginning to emerge (Donnelly et al., 2006). Recent work by Tuan et al. (2006) extended a quasi-2DV cross shore profile model of the nearshore called UNIBEST-TC (Bosboom et al., 2000; Roelvink and Stive, 1989; Stive and Wind, 1986) to include wave overwash and simulate the morphological development in a flume experiment. However, the only numerical model that has been validated for cross shore profile change under prototype runup overwash conditions is the 1D cross shore profile model SBEACH (Larson and Kraus, 1989;

* Corresponding author. Deltares, PO Box 177, 2600 MH, Delft, The Netherlands. Tel.: +31 15 2858706.
E-mail address: robert.mccall@deltares.nl (R.T. McCall).

0378-3839/$ – see front matter © 2010 Elsevier B.V. All rights reserved.
doi:10.1016/j.coastaleng.2010.02.006

Larson et al., 1990, 2004), which is based on the equilibrium sediment transport concept.

Although current cross shore profile overwash models provide useful predictions of 1D washover morphology, they are limited by the inherent assumption of longshore uniformity or longshore parameterization in forcing and bed profile. Field studies have shown that overwash is highly influenced by spatial variations in forcing and dune strength (Morton and Sallenger, 2003; Suter et al., 1982). Therefore it is important for any model to incorporate such longshore variation in order to successfully simulate overwash in a broad range of cases.

A second property of current overwash models that may limit their applicability is that they do not account for infragravity waves. Raubenheimer and Guza (1996) show that during storm conditions, infragravity swash is dominant over incident band swash on dissipative beaches. Near dune hydrodynamics are affected by both the incident band and infragravity waves (van Thiel de Vries et al., 2008). It is conceivable that infragravity waves also play a role during runup overwash and the initiation of inundation overwash, and should therefore be included in overwash models.

Roelvink et al. (2009) developed a new process-based and time dependent 2DH model of the nearshore and coast called XBeach. This model solves coupled equations for cross shore and longshore hydrodynamics and morphodynamics on the time scale of wave groups, including the generation of infragravity waves. The model allows for variation in hydrodynamic forcing and morphological development in the longshore dimension. The hydrodynamics and morphodynamics of XBeach have been extensively calibrated and validated against (1D) flume experiments (Roelvink et al., 2008, 2009; van Thiel de Vries, 2009), and some (2DH) field cases (Roelvink et al., 2009). In particular, the model showed qualitative skill in simulating dune erosion and overwash in measured cross shore profiles of Assateague Island, Maryland. Until present the model has not been validated using 2DH field cases with dune erosion and overwash.

In this paper we use XBeach to simulate 2DH overwash morphology on a barrier island during Hurricane Ivan. A section of Santa Rosa Island, Florida, is chosen that showed significant morphological response to the storm and was captured by high quality pre- and post storm LIDAR (Light Detection and Ranging, Brock et al., 2002) data. Sparse field data and large-scale numerical model results are used to produce parametric hydraulic boundary conditions for a base simulation. A comparison is made between measured and simulated bed level change on the island. Sensitivity simulations are carried out in which the base parametric hydraulic boundary conditions are varied to account for errors in the parameterization of the base boundary conditions. The results of these simulations are included to determine the accuracy of the model and to gain insight into the effect of hydraulic parameters on an overwash system. Sensitivity studies are also carried out to examine the sensitivity to two internal parameters and the results are used to indicate areas of further research.

Section 2 describes the fundamentals of XBeach. A description of the model area and available data are given in Section 3. The setup and results of the base XBeach simulation of Hurricane Ivan are discussed in Section 4 and Section 5. Section 6 discusses the sensitivity analysis. The conclusions of this paper are given in Section 7.

2. XBeach

XBeach is a 2DH (depth averaged) model that solves coupled short wave energy, flow and infragravity wave propagation, sediment transport and bed level change. The model has a robust numerical scheme (Stelling and Duinmeijer, 2003), allowing it to simulate flooding and drying, thereby removing the need for separate dry and wet domains and procedures. A brief description of the model is given below. A more comprehensive description is given by Roelvink et al. (2009).

2.1. Model equations

XBeach solves the time dependent short wave action balance on the scale of wave groups. The directional distribution of the short wave action density spectrum is taken into account in the model, whereas the frequency domain is represented by a single representative peak frequency, assuming a narrow banded incident spectrum (c.f. Goda, 1985). This approach is similar to the 2nd generation spectral HISWA model (Holthuijsen et al., 1989), but includes time-dependency. Using these wave action formulations it is possible to solve directionally-spread infragravity waves and time-varying currents, as will be described below.

The wave action balance is given as follows:

$$\frac{\partial A}{\partial t} + \frac{\partial c_{g,x} A}{\partial x} + \frac{\partial c_{g,y} A}{\partial y} + \frac{\partial c_\theta A}{\partial \theta} = -\frac{D_{\text{waves}}}{\sigma} \tag{1}$$

where $A = {}^{E}/_{\sigma}$, E is the wave energy and σ is the intrinsic wave frequency. The x- and y-velocities ($c_{g,x}$, $c_{g,y}$) in Eq. (1) represent the respective components of the wave group velocity. The velocity in directional space (c_θ) takes into account refraction due to bottom and currents. The energy dissipation due to wave breaking, D_{waves}, is modeled according to Roelvink (1993). XBeach includes a roller energy balance in order to redistribute energy from breaking waves to foam. Dissipation of short wave energy is used as a source term in the roller energy balance:

$$\frac{\partial E_{\text{roller}}}{\partial t} + \frac{\partial c_x E_{\text{roller}}}{\partial x} + \frac{\partial c_y E_{\text{roller}}}{\partial y} + \frac{\partial c_\theta E_{\text{roller}}}{\partial \theta} = -D_{\text{roller}} + D_{\text{waves}}. \tag{2}$$

Roller energy dissipation is calculated according to Reniers (1999), following Deigaard (1993) and Svendsen (1984).

Surface elevation and flow, including infragravity waves and unsteady wave-induced currents, are solved using the shallow water momentum and mass balance equations. To include short wave-induced mass fluxes and return flows in shallow water, XBeach uses the Generalized Lagrangian Mean formulation (Andrews and McIntyre, 1978). The depth-average GLM-shallow water equations are given as follows:

$$\frac{\partial u^L}{\partial t} + u^L \frac{\partial u^L}{\partial x} + v^L \frac{\partial u^L}{\partial y} - \nu_h \left(\frac{\partial^2 u^L}{\partial x^2} + \frac{\partial^2 u^L}{\partial y^2} \right) = -g \frac{\partial \eta}{\partial x} - \frac{c_f u^E \sqrt{(1.16 u_{\text{rms}})^2 + (u^E)^2 + (v^E)^2}}{h} + \frac{F_x}{\rho h} \tag{3}$$

$$\frac{\partial v^L}{\partial t} + v^L \frac{\partial v^L}{\partial y} + u^L \frac{\partial v^L}{\partial x} - \nu_h \left(\frac{\partial^2 v^L}{\partial y^2} + \frac{\partial^2 v^L}{\partial x^2} \right) = -g \frac{\partial \eta}{\partial y} - \frac{c_f v^E \sqrt{(1.16 u_{\text{rms}})^2 + (u^E)^2 + (v^E)^2}}{h} + \frac{F_y}{\rho h} \tag{4}$$

$$\frac{\partial \eta}{\partial t} + \frac{\partial u^L h}{\partial x} + \frac{\partial v^L h}{\partial y} = 0. \tag{5}$$

L- and E-indexes for the $x(u)$ and $y(v)$ velocities refer to Lagrangian and Eulerian framework. Water depth is denoted by h, the water surface elevation by η and the bed friction coefficient by c_f. The horizontal viscosity coefficient (ν_h) is modified by wave breaking in the surf zone, following Reniers et al. (2004). Bed friction is calculated using the parameterization of Feddersen et al.

(2000) using both the Eulerian flow velocities (u^E, v^E)and the short wave orbital velocity, calculated as:

$$u_{rms} = \frac{\pi H}{T\sqrt{2\sinh(kh)}} \tag{6}$$

where $H = \sqrt{\frac{8E}{\rho g}}$ is the wave height, T is the wave period and k is the wave number. The wave and roller forcing terms (F_x, F_y) in Eqs. (3) and (4) are calculated from the short wave radiation stress gradients in x- and y-direction, which are functions of the wave and roller energies.

Sediment transport rates are calculated as:

$$\begin{aligned} S_x &= hCu^E - D_s h\frac{\partial C}{\partial x} \\ S_y &= hCv^E - D_s h\frac{\partial C}{\partial y} \end{aligned} \tag{7}$$

in which C is the depth-averaged sediment concentration and D_s is the sediment diffusion coefficient. Sediment concentrations in the water column are modeled using a depth-averaged advection–diffusion scheme with a source-sink term based on an equilibrium sediment concentration (Galapatti and Vreugdenhil, 1985):

$$\frac{\partial hC}{\partial t} + \frac{\partial hCu^E}{\partial x} + \frac{\partial hCv^E}{\partial y} + \frac{\partial}{\partial x}\left(D_s h\frac{\partial C}{\partial x}\right) + \frac{\partial}{\partial y}\left(D_s h\frac{\partial C}{\partial y}\right) = \frac{hC_{eq} - hC}{T_s} \tag{8}$$

where T_s is the sediment concentration adaptation time scale. The equilibrium concentration source-sink term (C_{eq}) is calculated using the Soulsby–Van Rijn formulation (Soulsby, 1997):

$$C_{eq} = \frac{A_{sb} + A_{ss}}{h}\left(\sqrt{u^2_{stirring}} - u_{cr}\right)^{2.4} \tag{9}$$

$$u_{stirring} = \sqrt{(u^E)^2 + (v^E)^2} + 0.018\frac{u_{rms}}{C_d} \tag{10}$$

in which u_{cr} is the critical transport velocity based on Shields (see van Rijn, 1993), C_d is the short wave-related drag coefficient and A_{ss} and A_{sb} are suspended and bed load transport coefficients respectively.

It has been shown previously that XBeach will over predict overwash-driven morphological change when large amounts of sediment are suspended in the water column and the Shields number is high (McCall, 2008). Several explanations can be given for this over prediction, including the resistance effects of vegetation and soil cohesion and the choice of sediment transport relation. Since the model site is barely vegetated, it is expected that the greatest source of the over estimation of morphological change is the sediment transport relation.

Several studies have shown that standard empirical pick-up functions over predict erosion rates in the case of high sediment concentrations and Shield numbers exceeding 1 (van Rhee, 2007; van Rhee and Talmon, 2000). It is argued by Van Rhee (2007) and in a breach simulation by Bisschop et al. (2009) that this can be improved by including the resistance to erosion due to soil dilatancy. A reduction in the suspended sediment transport capacity due to turbulence damping caused by the sheet flow layer (Winterwerp, 2001) and reduced bottom shear stress in sheet flow conditions (Foster, D.L., pers comm.) may also explain in part the overestimation of sediment transport rates by standard pick-up functions. It is not within the scope of this paper to derive a sediment transport model for overwash conditions, but rather to model these processes correctly in a parametric way so that a realistic study of the hindcast of a storm and variations in hydraulic forcing can be made. In order to achieve this, the equilibrium sediment concentration in XBeach is limited during sheet flow. This approach assumes that in sheet flow conditions higher velocities lead to higher sediment transport rates, but not to higher equilibrium sediment concentrations, which is not necessarily correct. However, the limiting function does ensure that sediment transport under overwash conditions becomes a linear function of flow discharge, which is in line with Kobayashi et al. (1996). The transport constraint remains a proxy for other unknown or unrepresented factors. The effect of this proxy is discussed in the Sensitivity analysis section of this paper.

The limitation described above is placed on the equilibrium sediment concentration by limiting the Soulsby–Van Rijn stirring velocity during sheet flow:

$$u^2_{stirring} = \begin{cases} u^2_{stirring} & \theta_s < \theta_{sf} \\ \theta_{sf}\dfrac{gD_{50}\Delta}{c_f} & \theta_s \geq \theta_{sf} \end{cases} \tag{11}$$

$$\theta_s = \frac{c_f u^2_{stirring}}{\Delta g D_{50}} \tag{12}$$

where θ_s is the Shields parameter, θ_{sf} is the Shields parameter for the start of sheet flow (usually 0.8–1.0), Δ is the relative density of the sediment and D_{50} is the median grain size.

Bed level change due to sediment transport rate gradients is assumed to occur on a time scale that is much longer than those associated with the hydrodynamic processes. Therefore, the time scale for the morphologic changes can be accelerated such that they take place at a rate that is still slower than the hydrodynamic processes, but occur rapidly enough to be relevant over a small number of hydrodynamic cycles. Thus:

$$\frac{\partial z_b}{\partial t} + \frac{f_{mor}}{(1-p)}\left(\frac{\partial S_x}{\partial x} + \frac{\partial S_y}{\partial y}\right) = 0 \tag{13}$$

in which f_{mor} is a morphological acceleration factor of O(1–10) and p is the bed porosity.

XBeach uses an avalanching algorithm in order to simulate dune slumping during storm conditions. Avalanching occurs if the bed slope exceeds a prescribed critical value for wet or dry points, as extensively tested by Van Thiel de Vries (2009).

In XBeach surge level time series can be applied to all four corners of the model domain. Wave forcing can only be applied on the offshore boundary. XBeach allows the generation of spatially, directionally and temporally varying irregular wave groups and associated bound infragravity waves, based on an input short wave spectrum. The technique used in XBeach is based on the theory of Hasselmann (1962; c.f. Herbers et al., 1994), previously used by Van Dongeren et al. (2003) to model infragravity waves during the DELILAH campaign with a SHORECIRC model (Svendsen et al., 2002; van Dongeren et al., 1994). An absorbing-generating boundary condition developed by Van Dongeren and Svendsen (1997) allows infragravity waves to propagate freely out of the model on the offshore or back barrier bay boundary with minimal reflection. Neumann boundary conditions are applied for the flow, short wave energy and sediment transport on the lateral (shore normal) boundaries.

3. Hurricane Ivan and Santa Rosa Island

Hurricane Ivan was the largest of five hurricanes to strike the US coast in 2004, ranking as the tenth most powerful Atlantic hurricane on record. Hurricane Ivan made landfall at 06:50 UTC on 16 September just east of Mobile Bay, Alabama, as a category 3 hurricane on the Saffir–Simpson scale. The damage to properties and infrastructure caused by Hurricane Ivan is estimated at $14.6 billion (National Hurricane Center, 2008).

Santa Rosa Island, FL, is a wave dominated, narrow barrier island between the Gulf of Mexico and the Santa Rosa Sound on

the Northern Florida Panhandle. The island is aligned approximately east–west and has a length of roughly 85 km. The width of the island varies between 150 and 1000 m. The western-most tip of the island is approximately 50 km from the location of landfall of Hurricane Ivan, see Fig. 1. During Hurricane Ivan, large stretches of Santa Rosa Island were overwashed. Overwash deposit depths up to 1.5 m and multiple breaches occurred on the western-most tip (Department of Environmental Protection State of Florida, 2004).

The site studied in this paper is a two-kilometer stretch of Santa Rosa Island between Pensacola Beach and Navarre Beach, which is part of the Gulf Islands National Seashore, see Figs. 1 and 2. The area was heavily overwashed during Hurricane Ivan as can be seen in the aerial photographs in Fig. 3.

3.1. Available bathymetric and altimetric data

Two LIDAR surveys of the study area carried out on 15 May 2004 and 19 September 2004 provide high resolution pre- and post-storm bathymetry and altimetry data of the study area. The LIDAR measurements prior to Hurricane Ivan span most of the width of Santa Rosa Island and much of the nearshore; see Fig. 4 (left panel). Post Hurricane Ivan LIDAR data are less complete than the pre-storm data. Only one swath was made in order to quickly assess the state of the dunes. Much of the bay side of the island was not surveyed, along with the nearshore on the Gulf side; see Fig. 4 (center panel). Analysis of the pre- and post-storm data reveals patterns of erosion and deposition which are mainly due to the smoothening of the initially irregular profile during the storm. These patterns are shown in Fig. 4 (right panel). The mean bed level change caused by the storm was 0.09 m of erosion and the standard deviation of bed level change was 0.74 m. Changes in dune height of several meters were observed.

Pre-storm bathymetry data of the back bay area are extracted from the NGDC Coastal Relief Model (Divins and Metzger, 2008). These data are combined with the pre-storm LIDAR data by means of scale-controlled interpolation (Plant et al., 2002) to generate the pre-storm bed elevation for the model; see Fig. 5.

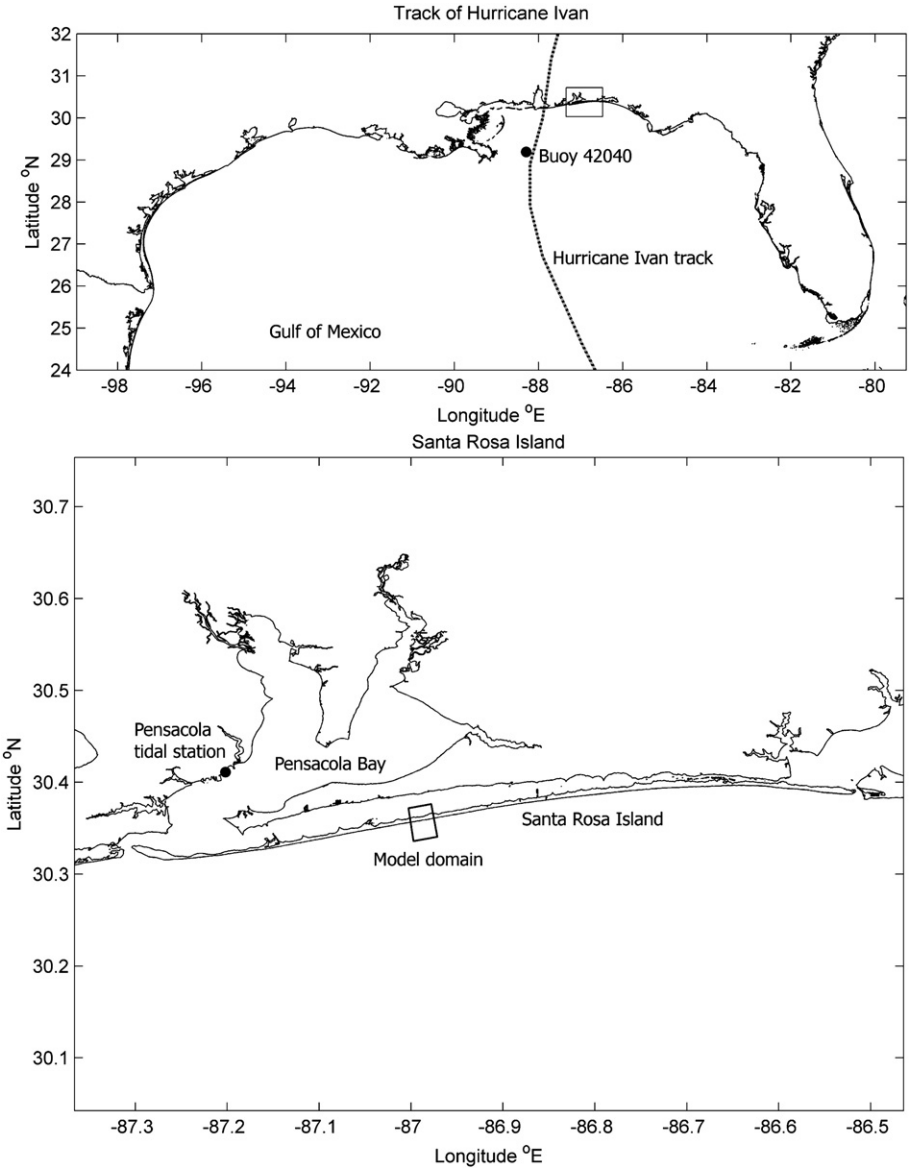

Fig. 1. Top panel: Track of Hurricane Ivan (dash–dot) based on data from National Hurricane Center (2008). The area in the inner box is shown in the bottom panel. The Pensacola tidal station and NOAA-NDBC buoy 42040 are shown in the bottom and top panels respectively.

3.2. Available wave data

No nearshore or shallow water in-situ wave measurements exist for the study area on Santa Rosa Island during Hurricane Ivan. As Hurricane Ivan approached land, several NOAA wave buoys measured wave heights in deep water. The wave conditions at these wave buoys are expected to be more extreme than the conditions at the relatively shallow water offshore boundary of the XBeach model and therefore cannot be used directly. However, these buoy data were used to calibrate a large-scale numerical wave model (SWAN, Booij et al., 1999), which was forced using three hourly Hwind and NARR wind field datasets provided by NOAA Hurricane Research Division of AOML, NOAA National Climatic Data Center and NOAA National Centers for Environmental Prediction. A comparison between the measured wave conditions at NOAA-NDBC buoy 42040 (near the path of Hurricane Ivan, see Fig. 1) and those simulated in the SWAN model is given in Fig. 6.

The results show that although the SWAN model used in this study does not have perfect skill, the results of the SWAN model may be used to give reliable indicative values for the significant wave height and peak wave period at the boundary of the XBeach model, 1.5 km offshore of Santa Rosa Island. At this location the significant wave height during the storm varies from 2.5 m to 7.0 m, with peak wave periods decreasing from 20 s to 10 s as the storm progresses.

3.3. Available surge data

The National Oceanic and Atmospheric Administration (NOAA) has one tidal gauge near Santa Rosa Island at Pensacola that was measuring during Hurricane Ivan. The gauge is located within Pensacola Bay behind Santa Rosa Island, see Fig. 1, and stopped measuring during the peak of the storm, when the water level reached 2.1 m + MSL, see Fig. 7. The measured water level at this location cannot be used directly to impose a surge level on the offshore boundary of the XBeach model as the geometry and depth of Pensacola Bay is likely to modify and possibly enhance the surge level compared to the surge level offshore of Santa Rosa Island. It may be assumed however that the surge level offshore Santa Rosa Island will not exceed the maximum recorded surge level at Pensacola tidal gauge. Measured post-storm high water marks measured near the study area at Pensacola Beach and Navarre Beach indicate maximum water levels of 2.8 m–3.5 m + MSL over the island (Wang and Manausa, 2005). Based on empirical runup relations, Wang et al. (2006) estimate that approximately half of the total high water mark level along the northwestern Florida barrier coast during Hurricane Ivan was caused by wave setup and runup, indicating that the offshore surge level at Santa Rosa Island may have reached 1.75 m + MSL.

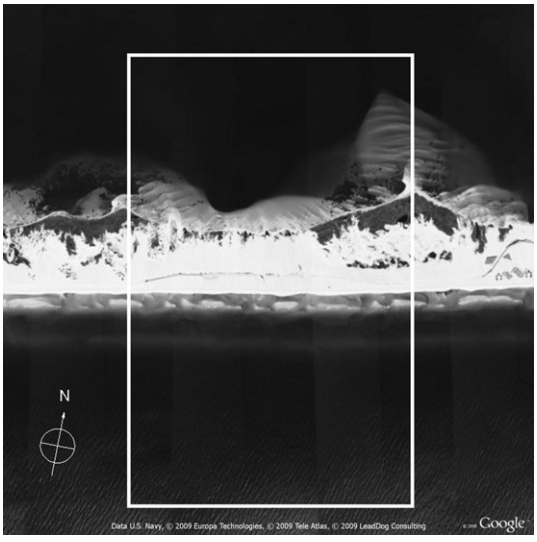

Fig. 2. December 2004 aerial photo of the study site [image courtesy of Google Earthmapping service]. Rectangle indicates the model domain.

4. Model setup

The initial bed level for the XBeach model is based on the combined pre-storm LIDAR and NGDC elevation data described in the previous section. The XBeach model requires boundary conditions for the offshore wave conditions and the surge level time variation. The wave and surge data described in the previous section represent a reasonable estimate of the true conditions during the hurricane, considering that there are no measurement data with which to validate the local hydraulic conditions at Santa Rosa Island. The estimates can however be expected to contain errors and should therefore be dealt with appropriately. Since there are no time series of the surge level at Santa Rosa Island, the surge and wave conditions will be described in a parametric way, based on the available surge and wave data. This base parameterization is described below. The model results using this base parameterization are compared to the measured LIDAR post-storm elevation data, which is discussed in detail in the "Model results" section. In order to compensate for errors in the boundary condition parameterization and for errors in the available wave and surge data, sensitivity studies are carried out in which the hydraulic forcing is varied. These studies are described in the Sensitivity analysis.

4.1. Base parametric boundary conditions

Based on the duration of high energy wave conditions, the duration of the storm is set at 36 h. The wave conditions on the offshore boundary of the XBeach model are described by a JONSWAP shape in the frequency domain. The significant wave height varies from 2.5 m to 7.0 m, based on the SWAN wave model results discussed earlier. The wave height time series is centered symmetrically round the peak of the surge, see Fig. 8 (first panel). The peak wave period on the offshore boundary decreases during the storm from 20.0 s to 10.0 s, mimicking the frequency dispersion of the hurricane-generated waves in the SWAN wave model; see Fig. 8 (second panel). The surge level in the simulation varies from high astronomical tide, 0.30 m + MSL, to 1.75 m + MSL, based on the maximum estimate of the high water marks described earlier. The surge level is assumed symmetrical around the peak of the storm. The surge level time series imposed on the offshore boundary of the XBeach model is shown in Fig. 8 (third panel). Since there are no data to describe the surge level directly behind Santa Rosa Island, the surge level on the bay side of the XBeach model is assumed identical to the surge level on the offshore boundary of the model; see Fig. 8 (fourth panel). This assumption may not be correct, as Santa Rosa Island may have acted as a barrier for the surge. The effect of this assumption is discussed in the Sensitivity analysis.

4.2. Model parameters

The XBeach model has a number of free parameters which can be used to calibrate the model. These govern parameterizations in the short wave hydrodynamics, flow, sediment transport and bed update. Since no measurements exist in order to calibrate the hydrodynamics of the model, default values for this version of XBeach are used for the short wave hydrodynamics and flow (see Appendix). The default critical dry and wet slope angles for avalanching are 1.0 and 0.15 respectively, following the analysis of Van Thiel de Vries (2009). The median sediment diameter is estimated at 0.2 mm, corresponding with values found by Claudino-Sales et al. (2008). The Shields value at

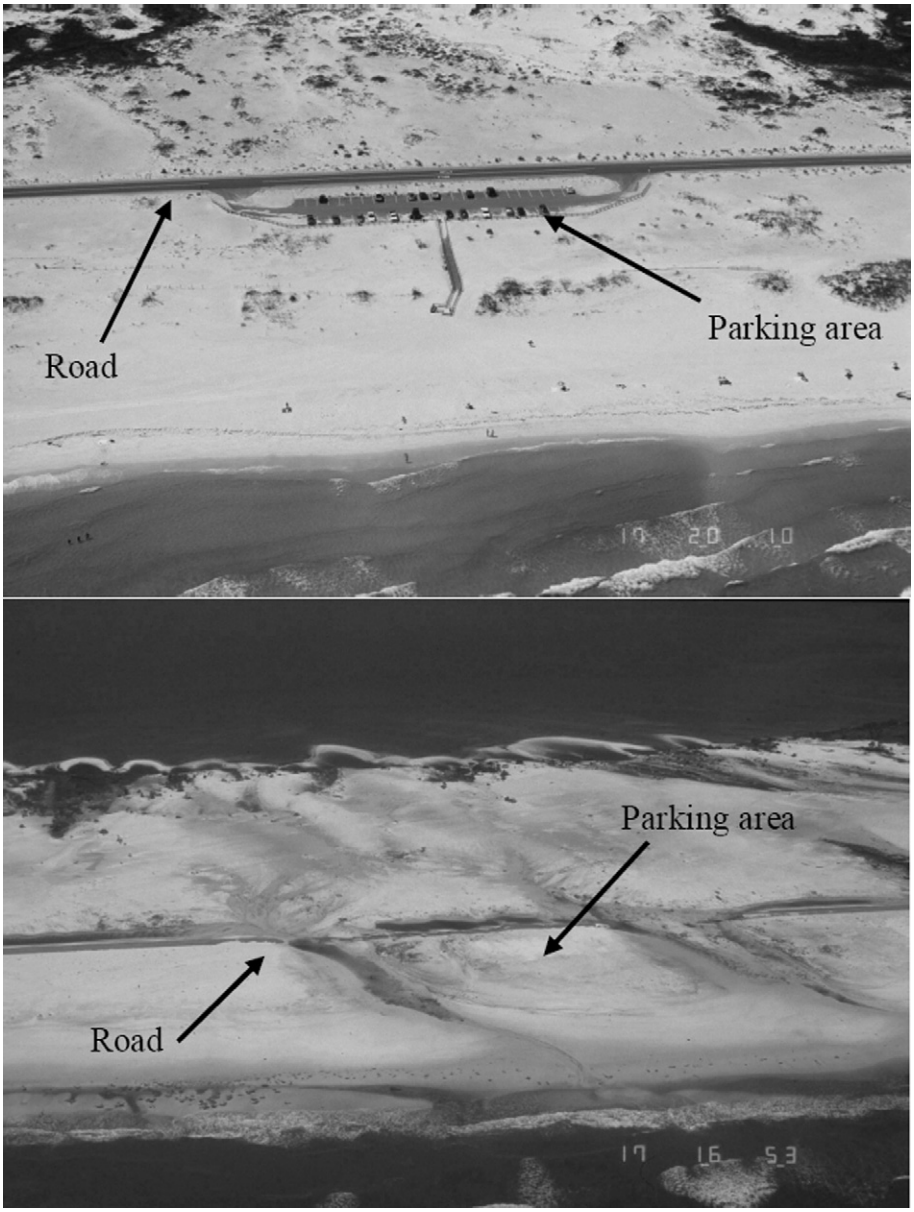

Fig. 3. Aerial photo of the model location in July 2001(top panel) and 19 September 2004, three days after Hurricane Ivan (bottom panel). Image courtesy of USGS.

which the sheet flow transport limiter is applied (θ_{sf}) has no previously defined default value, but should correspond with the start of sheet flow. In this simulation θ_{sf} is set to 1.0. This value is varied in the sensitivity analysis. A morphological acceleration factor of 10 is introduced to decrease calculation time. The effect of this factor is also discussed in the Sensitivity analysis. Grid spacing in the longshore direction is set at 20 m. In the cross shore direction the grid spacing varies from 2 m across the barrier island to 29 m on the offshore boundary.

5. Model results

The base simulation can be divided into three stages based on the hydrodynamic forcing and morphological change. These three stages of morphological change correspond well with the collision, runup and inundation regimes of the Storm Impact Scale developed by Sallenger (2000). In the first 6 h of the simulation the barrier island is in the collision regime. The surge level and wave heights are low and the combined surge and wave runup does not exceed the height of the foredunes, see Fig. 9 (upper left panel). Therefore the morphological response is limited primarily to erosion of the foredunes and deposition in the nearshore area (Fig. 10, second panel). The second stage, or runup regime, runs from approximately the sixth to the twelfth hour. During this time the surge level and wave height increase, leading to runup overwash (Fig. 9, upper right panel). Further erosion of the foredunes takes place, as well as small amounts of erosion and deposition on the back barrier (Fig. 10, third panel). From the twelfth hour onwards the combined surge level and wave setup exceeds the height of the foredunes, which are already reduced in height by the preceding phases of the storm, leading to inundation overwash (Fig. 9, bottom left panel). The maximum hourly-mean velocities across the barrier island are supercritical. Shields values on the back barrier during this period are in the order of 9. Large amounts of sediment are transported from the foredunes to the back barrier and back barrier bay. Two distinct washover fans, see Fig. 10 (fourth panel), are created in the back barrier bay. A large area of the barrier island remains inundated until the final hours of the simulation.

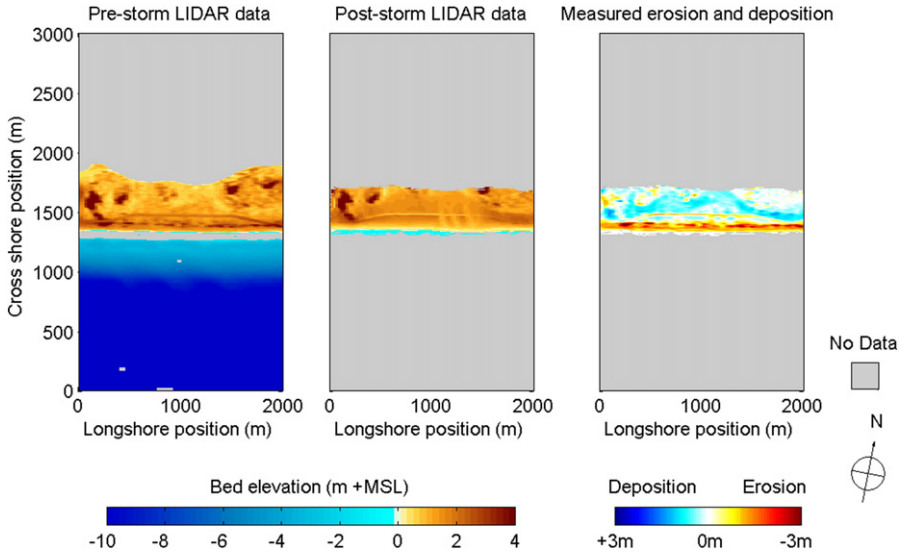

Fig. 4. LIDAR-measured bed elevation of the study site on 15 May 2004 (left panel), LIDAR-measured bed elevation of the study site on 19 September 2004 (center panel) and erosion–deposition plot based on the pre- and post-storm LIDAR data (right panel).

The simulated and measured post-storm regions of erosion and deposition around the barrier island are shown in Fig. 10 (fourth and fifth panels respectively). Note that the post-storm measured data are limited to a section of the subaerial barrier island and that the simulated development of the nearshore and back barrier bay cannot be compared to measured data. The LIDAR measurements show erosion in the order of 1–3 m of the foredunes. Deposition in the order of 1 m on the back barrier takes place along three deposition channels, the locations of which appear to be determined by the presence of large dune features on the back barrier, which survive the hurricane. The simulated erosion and deposition pattern in the base XBeach model corresponds favorably to the measured pattern. In the model, erosion takes place around the foredunes and deposition takes place in the same three deposition channels as in the measured data. The magnitude of both the erosion and deposition on the barrier island appears to be less in the base XBeach simulation than in the measurement data.

A comparison of three distinct measured and modeled post-storm profiles is given in Fig. 11. The profiles show that foredune lowering is captured well by the model, both for high foredunes (bottom panel) and for low foredunes (top and center panels). The model also correctly predicts limited lowering of back barrier dunes (top panel). As also shown by Fig. 10 (fourth panel), the model under predicts the deposition on the back barrier.

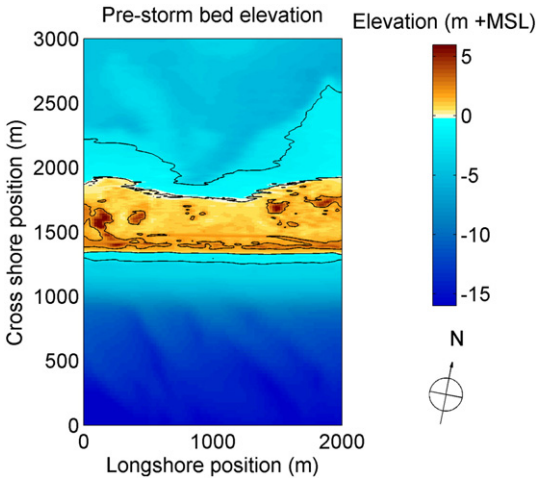

Fig. 5. Initial bed elevation of the model created from the combined pre-storm LIDAR and NGDC elevation data. Contour lines refer to −2 m, 0 m and +2 m + MSL.

A quantification of the skill of the model is required in order to determine whether the model can be used as a significantly useful predictive tool. One measure of skill is to compare the simulated error in bed level change to the variance of the observed bed level change at all locations where pre- and post-storm data were sampled. The skill is defined as (Gallagher et al., 1998):

$$Skill = 1 - \frac{\sum_{i=1}^{N} \left(dz_{b_{LIDAR,i}} - dz_{b_{XBeach,i}} \right)^2}{\sum_{i=1}^{N} \left(dz_{b_{LIDAR,i}} \right)^2} \tag{14}$$

where N is the number of data points covered by both pre- and post-storm LIDAR measurements, $dz_{b_{LIDAR,i}}$ is the measured bed level change in point i and $dz_{b_{XBeach,i}}$ is the modeled bed level change in point i. If the skill is equal to one, the simulation is perfect. If it is zero, the simulation is no better than predicting zero bed level change. If the skill is less than zero, the simulation is worse than predicting zero bed level change.

In most applications, the skill is not expected to be equal to one. In this case, the errors in the model results include both random components and a persistent bias. The mean error describes the potential bias and is calculated as follows:

$$Bias = \frac{1}{N} \sum_{i=1}^{N} \left(z_{b_{post-storm,XBeach,i}} - z_{b_{post-storm,LIDAR,i}} \right). \tag{15}$$

The skill and bias calculated for the base XBeach simulation and a zero bed level change prediction are given in Table 1. It can be seen that XBeach has considerable skill in predicting the bed level change. This shows that XBeach represents the variance in bed level change well. The base XBeach simulation predicts on average a 0.13 m lower bed level in the region of LIDAR data than found in the measurement data. This is reflected in the bias of the base XBeach simulation. This bias, although larger than the bias of a zero bed level change prediction, remains much smaller than the measured standard deviation

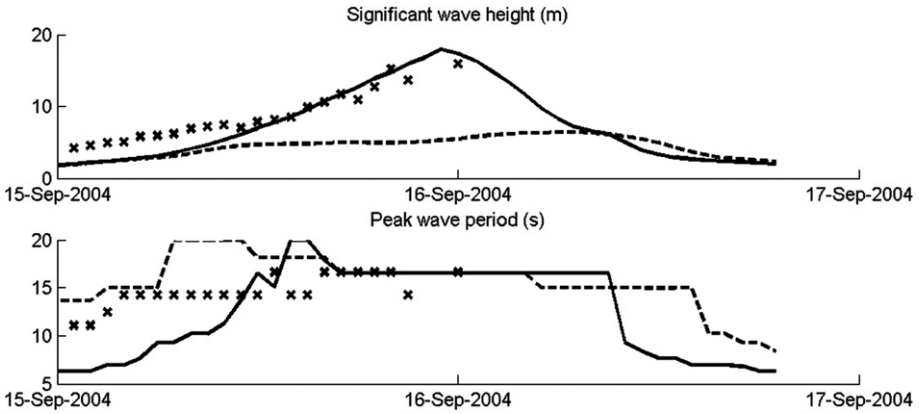

Fig. 6. NDBC measured (crosses) and SWAN simulated (solid line) significant wave height (top panel) and peak wave period (center panel) at NOAA-NDBC buoy 42040. SWAN simulated significant wave height and peak wave period at the offshore edge of the XBeach model are shown by the dotted line.

of the bed level change (0.74 m) and is comparable in magnitude to GPS navigation errors in the LIDAR data.

The error in the predicted bed level change is examined further in Fig. 12. In this figure the modeled bed level change is plotted versus the measured bed level change for every point in the model for which pre- and post-storm LIDAR data are available. The color scale in the plot indicates the density of points. It can be seen that the majority (96%) of points fall within one standard deviation of the measured bed level change from a perfect prediction. The distribution is weighted towards greater vectoral bed level change, i.e. more erosion or less deposition, in the model than in the measurements, which corresponds with the bias calculated previously. The figure shows that the accuracy of the modeled bed level change increases as the amount of measured erosion increases. It should be noted that the skill of the model has been determined by a point-to-point comparison. The effect of a horizontal translation of the modeled erosion and deposition pattern with respect to the measured pattern has not been examined.

6. Sensitivity analysis

In order to study the effect of uncertainties in hydraulic forcing and model parameters on the amount and patterns of erosion and overwash deposition, a series of sensitivity cases are examined. For each sensitivity case one parameter is varied relative to the simulation described in the previous section, referred to as the base case. The amount by which the hydraulic forcing parameters are varied is based on an estimate of the predictive error of the SWAN wave model and surge level hindcast. The effect of the variations on the predictive skill and bias will demonstrate how sensitive the model is to input settings and conversely how well the input values need to be known in order to yield useful predictions of morphological change. It should be noted that the skill and bias are based on the measured pre- and post-storm LIDAR data, which only covers part of the barrier island. The measures of bias and skill will therefore not reflect the entire difference in morphological response across the island, including the development of the washover fans. In order to give qualitative insight into the difference in the morphological response of the barrier island to each of the hydraulic forcing sensitivity cases, an analysis is made of the morphologically active area of the model. This area is divided into four zones. The first is the foreshore, which is defined as the area located in the Gulf of Mexico between −12 m and 0 m + MSL. The second zone is the foredune area, which extends from the shoreline to the + 1.5 m contour line immediately behind the foredunes (approximately 150 m into the barrier island). The back barrier zone extends from the foredunes to the waterline on the bay side of the island. This zone includes the higher dunes found on the back of the island. The fourth zone is the back barrier bay, which extends from the shoreline on the bay side of the island to the back boundary of the model. The change in volumes over time in each of these four zones will be presented for each hydraulic forcing sensitivity case.

6.1. Wave forcing sensitivity

In the first series of hydraulic sensitivity cases, the short wave forcing is varied while all other hydrodynamic conditions are kept constant. The parameters that are varied are the incident significant wave height and incident peak period. The incident wave height and

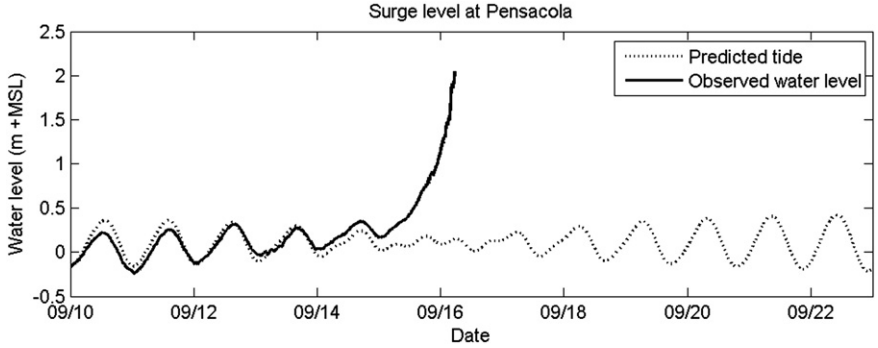

Fig. 7. Measured water level (solid line) and predicted astronomical tide (dotted line) at Pensacola.

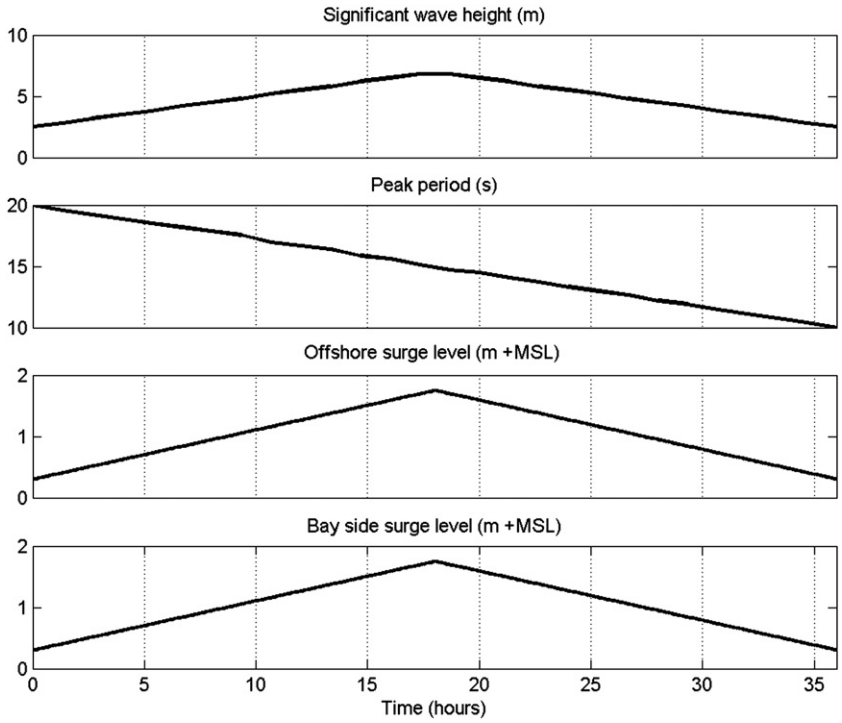

Fig. 8. Significant wave height (first panel) and peak wave period (second panel) on the offshore boundary and the still water surge level on the offshore (third panel) and bay side boundary (fourth panel) for the parametric base storm.

period are well known to affect the amount of foreshore erosion (e.g. Dean, 1977; Fischer and Overton, 1984; van Gent et al., 2008; Vellinga, 1986) and the energy in the infragravity wave band (e.g. Guza and Thornton, 1982). The values by which the input wave parameters vary relative to the base case are given in Table 2. The skill and bias of each sensitivity study is shown in the same table.

The morphological development of all four zones over time for all wave forcing variation cases are shown in Fig. 13. The figure shows that variations in wave height and wave period affect all four zones. In all cases, the foreshore, back barrier and back barrier bay accumulate sediment, which is provided for by a loss of sediment in the foredune zone. An increase in incident wave height or wave period both lead to greater amounts of foredune erosion. Changes in wave period affect the foreshore and foredune development from very early in the storm, whereas variations in wave height lead to different foreshore and foredune development after approximately 10 h. This may be because

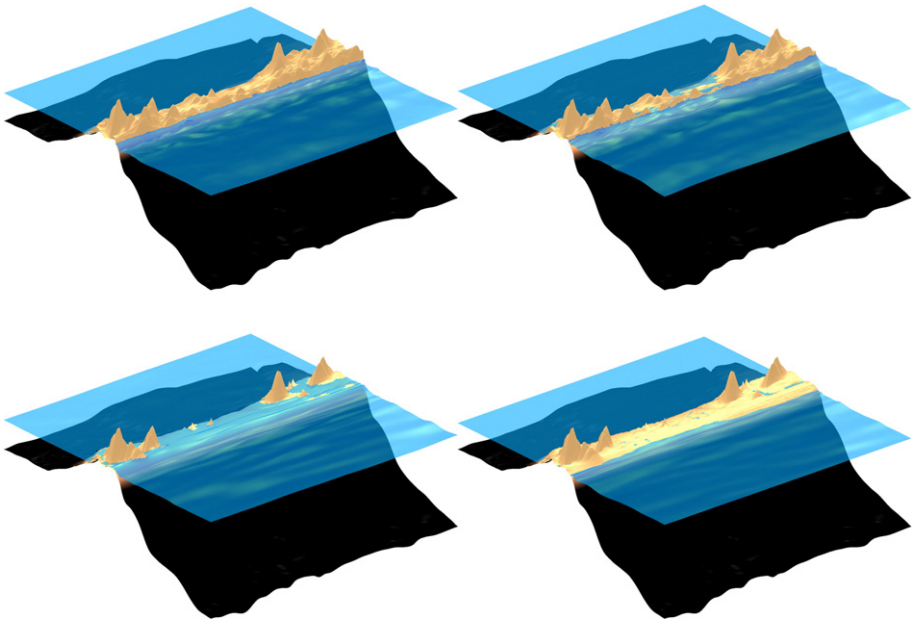

Fig. 9. Snapshot of the water level and bed elevation during the collision regime (top left panel, 3 h into the simulation), the overwash regime (top right, 8 h into the simulation), the inundation regime (bottom left, 30 h into the simulation) and at the end of the simulation (bottom right, 36 h into the simulation). The Gulf of Mexico is in the lower right and the back barrier bay in the upper left of all four panels.

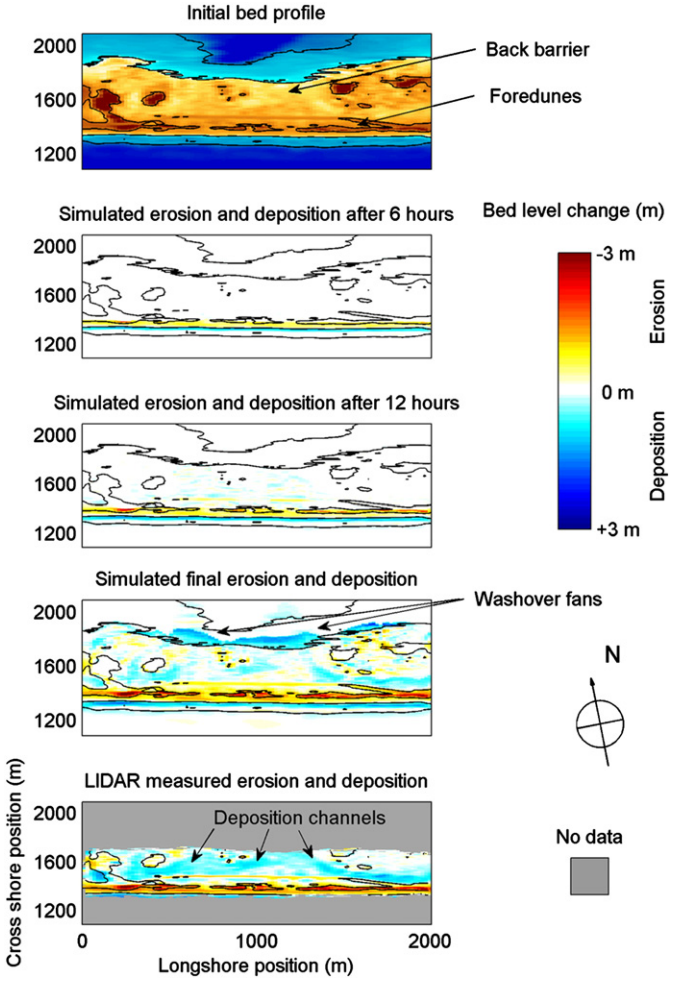

Fig. 10. Initial bed profile around the barrier island (first panel). Simulated erosion and deposition patterns after 6 h (second panel), after 12 h (third panel) and after 36 h (fourth panel). Measured regions of erosion and deposition (fifth panel). Contour lines refer to the pre-storm −2 m, 0 m and +2 m + MSL bed elevation.

Table 1
Skill and bias of the simulated post-storm barrier island elevation compared to the skill and bias of a zero bed level change prediction.

	Skill	Bias (m)
XBeach	0.74	−0.13
No change	0	+0.09

the base incident wave height is small at the start of the storm and thus the variations in wave height are not significant at this stage. Shorter wave periods lead to less erosion of the foredunes and more erosion of the nearshore (shore steepening relative to the base case) and longer wave periods lead to more erosion of the foredunes and less erosion of the nearshore (shore flattening). The start of development on the back barrier, which can be seen as the start of overwash, is determined strongly by the incident wave height and wave period. Development on the back barrier starts as deposition, but changes later to erosion. The periods during which erosion and deposition on the back barrier take place are dependent on the incident wave conditions, with larger wave heights and longer wave periods leading to an earlier switch from deposition to erosion. The development over time of the back barrier and back barrier bay in the wave height sensitivity case variations is almost identical to the development in the wave period sensitivity cases. Both the incident wave height and wave period are positively correlated to the amount of deposition in the back barrier bay and erosion of the back barrier. If the incident wave height or wave period is increased, the washover fans extend approximately 50 m farther into the bay than in the base case. A decrease in wave height and period lets the washover fans extend approximately 50 m less into the bay than in the base case.

6.2. Surge forcing sensitivity

The second series of hydraulic sensitivity cases consists of varying surge forcing while maintaining the base case wave forcing. The overall surge level and the surge level gradient across the barrier island are examined in separate cases. The overall surge level

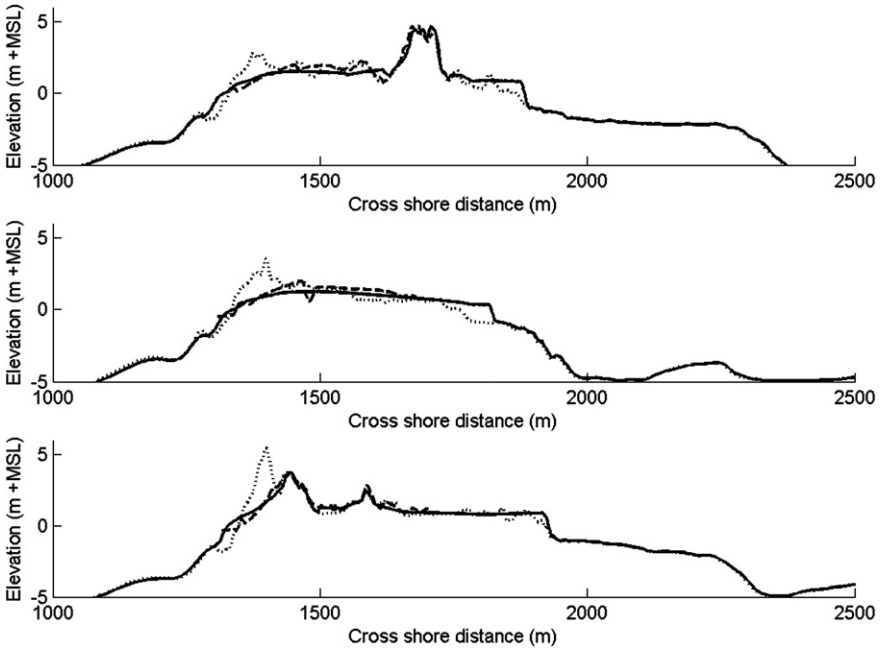

Fig. 11. Initial (dotted), measured post-storm (dashed) and modeled post-storm (solid) cross shore profiles for an area with low foredunes and a high back barrier dune (top panel, located at 500 m longshore distance), an area with low foredunes (center panel, located at 1000 m longshore distance) and an area with high foredunes (bottom panel, located at 1800 m longshore distance).

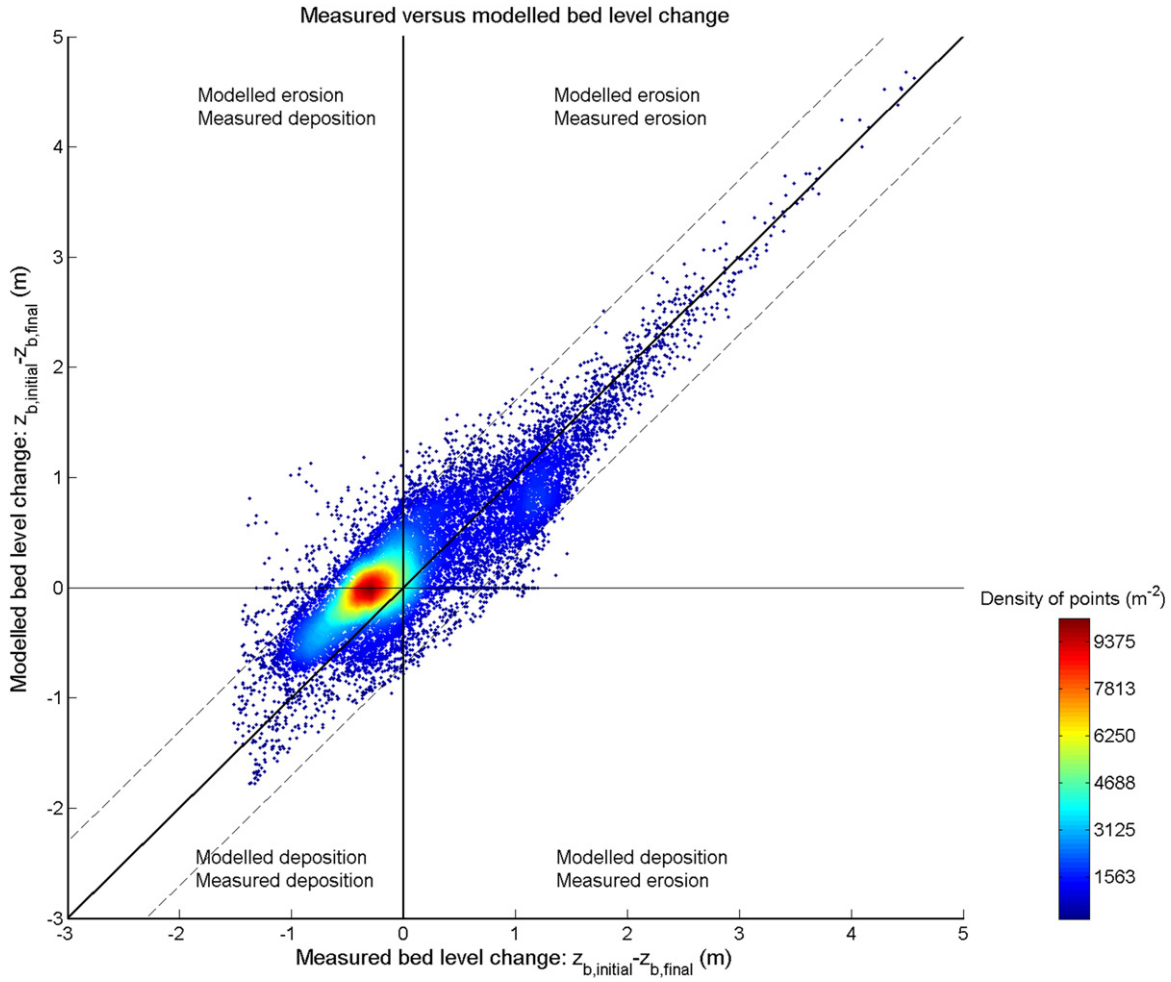

Fig. 12. Modeled bed level change versus measured bed level change for all points covered by pre- and post-storm measurement data. The thick solid line indicates a perfect 1:1 relation. The thin dashed lines indicate one standard deviation of the measured bed level change from the 1:1 relation. The color scale indicates the density of points in the plot.

determines to a great extent the storm response regime of the barrier island (Sallenger, 2000) and contributes to the amount of short wave energy available to erode the foreshore. The surge level gradient is known to influence the velocities on the back barrier during overwash (e.g. Donnelly et al., 2006; Suter et al., 1982). The influence of the overall surge level is investigated by increasing and decreasing the offshore and bay side surge levels simultaneously. The effect of the surge gradient across the barrier island is examined by increasing and decreasing the bay side surge only (constant direction of gradient) and by varying the phase shift between the offshore and bay side surge (varying direction of gradient). The values by which the sensitivity cases are varied relative to the base case are given in Table 3. The skill and bias of each sensitivity study is shown in the same table.

The development of the four morphological zones over time for all six surge variation cases are shown in Fig. 14. The figure shows that the foreshore and foredune development is only affected by variations in the overall surge level. This is to be expected as the other surge variations only affect the surge level in the back barrier bay. The overall surge level variation leads to differences in the development of the foreshore that are in the same order as differences caused by wave height and wave period variations. The change in foredune development due to surge level variations is smaller than that caused by incident wave variations. The start of overwash is affected little by the surge level variations. Once overwash has started however, a higher overall surge level leads to more deposition on the back barrier. The development of the back barrier and back barrier bay are strongly affected by surge level variations, particularly the back barrier bay surge level. A positive onshore surge level gradient (higher bay side surge) leads to more sediment deposition on the back barrier and less deposition in the back barrier bay, probably because of lower velocities on the back barrier. The results of the 2- and 4-hour surge delay cases show more deposition on the back barrier and less in the back barrier bay than the base case. This suggests that the positive surge level gradient in the second half of the simulation is more morphologically important than the negative surge level gradient in the first half of the simulation. The increase in model skill with higher bay surge levels and bay surge level delays indicate that the assumption of identical offshore and bay surge levels may not be

Table 2
Wave forcing sensitivity cases.

Wave sensitivity cases			
Name	Change relative to base case	Skill	Bias (m)
Base	–	0.74	−0.13
Higher wave height	Wave height +30%	0.68	−0.19
Lower wave height	Wave height −30%	0.73	−0.06
Higher wave period	Wave period +30%	0.66	−0.20
Lower wave period	Wave period −30%	0.69	−0.04

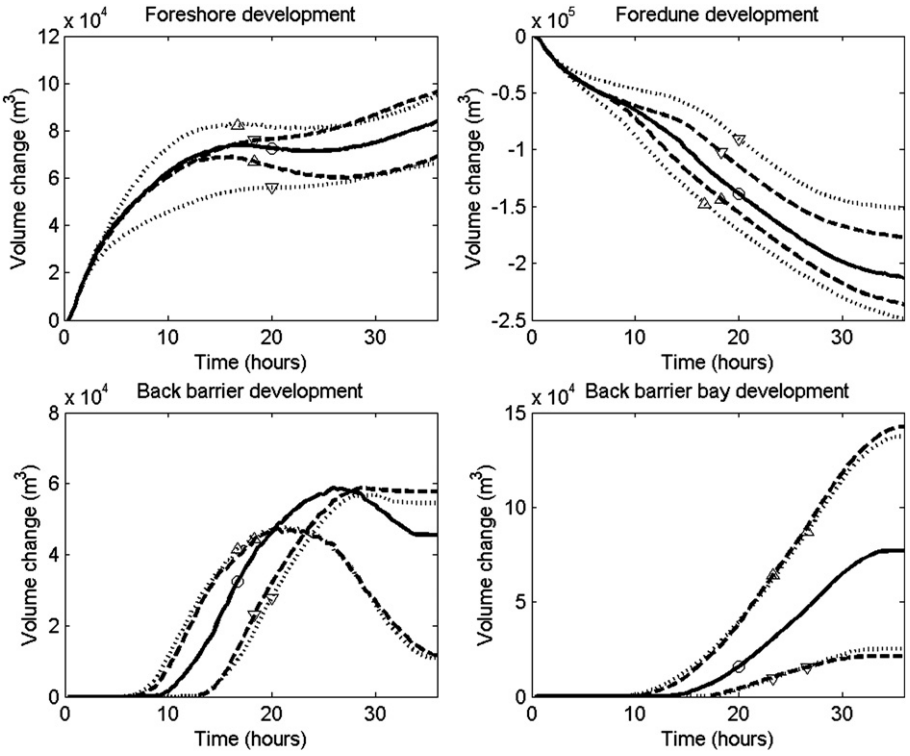

Fig. 13. Morphological development per region for the base simulation (solid line, circle), higher wave height case (dashed line, up-triangle), lower wave height case (dashed line, down-triangle), higher wave period (dotted line, up-triangle) and lower wave period (dotted line, down-triangle).

correct. In this simulation however, the quantitative effect of this error on the morphology in the area covered by post-storm LIDAR data is marginal.

6.3. Storm duration sensitivity

In the third series of hydraulic sensitivity cases the effect of the storm duration is examined. The wave and surge forcing are kept the same as in the base case, but the time frame in which they occur is increased or decreased in order to come to different total storm durations. The difference between the base case and the storm duration sensitivity cases is given in Table 4. The skill and bias of each sensitivity study is shown in the same table.

The development of the four morphological zones over time for the storm duration variation cases is shown in Fig. 15. The figure shows that all four zones are sensitive to the total duration of the storm. If the storm is lengthened, the amount of sediment eroded from the foredunes increases and more sediment is deposited in the foreshore and back barrier bay. This suggests that the barrier island, with the possible exception of the foreshore, does not reach an equilibrium storm profile in the model during the period of the storm. In the shorter duration case, more deposition takes place on the back barrier than in the base case. The reason for this may be that the back barrier area is sheltered for a relatively longer period behind the foredunes.

6.4. Model parameter sensitivity

Most model parameters have been kept at the default value for the base case and the hydraulic forcing sensitivity cases. The sensitivity of the model to these parameters will not be examined further. In the first set of model parameter sensitivity cases, the effect of the sheet flow sediment transport limiter (Eq. 11) is examined. The hydraulic boundary conditions and other model parameters are kept the same as in the base case. The difference between the transport limiter sensitivity cases and the base case is given in Table 5. In the second set of model parameter sensitivity cases, the effect of the morphological acceleration factor (Eq. 13) is investigated. The difference between the morphological acceleration sensitivity cases and the base case is also given in Table 5. The skill and bias of each sensitivity study is shown in the same table.

The morphological acceleration cases show that the model is insensitive to the imposed morphological acceleration factor. The model is more sensitive to the sheet flow sediment transport limiter. If the Shields value for the start of sheet flow transport limitation is varied around one ($\theta_{sf} = 0.8 - 1.2$), the skill and the bias of the model remain within the range found by variation of the hydraulic forcing parameters. This suggests that within this range the sheet flow transport limiter does not affect the final model results to a very great extent. However, if no transport limitation is applied, the skill and bias of the model are an order of magnitude worse than the other model results. The model predicts large amounts of erosion across the barrier island that are not seen in reality or the base simulation, see Fig. 16.

Table 3
Surge forcing sensitivity cases.

Surge sensitivity cases			
Name	Change relative to base case	Skill	Bias (m)
Base	–	0.74	−0.13
Higher surge	Offshore and bay side peak surge +25% (0.435 m)	0.73	−0.14
Lower surge	Offshore and bay side peak surge −25% (0.435 m)	0.74	−0.11
Higher bay surge	Bay side peak surge only +25% (0.435 m)	0.77	−0.09
Lower bay surge	Bay side peak surge only −25% (0.435 m)	0.72	−0.15
4-hour surge delay	Bay side surge lags behind offshore surge by 4 h	0.75	−0.12
2-hour surge delay	Bay side surge lags behind offshore surge by 2 h	0.75	−0.12

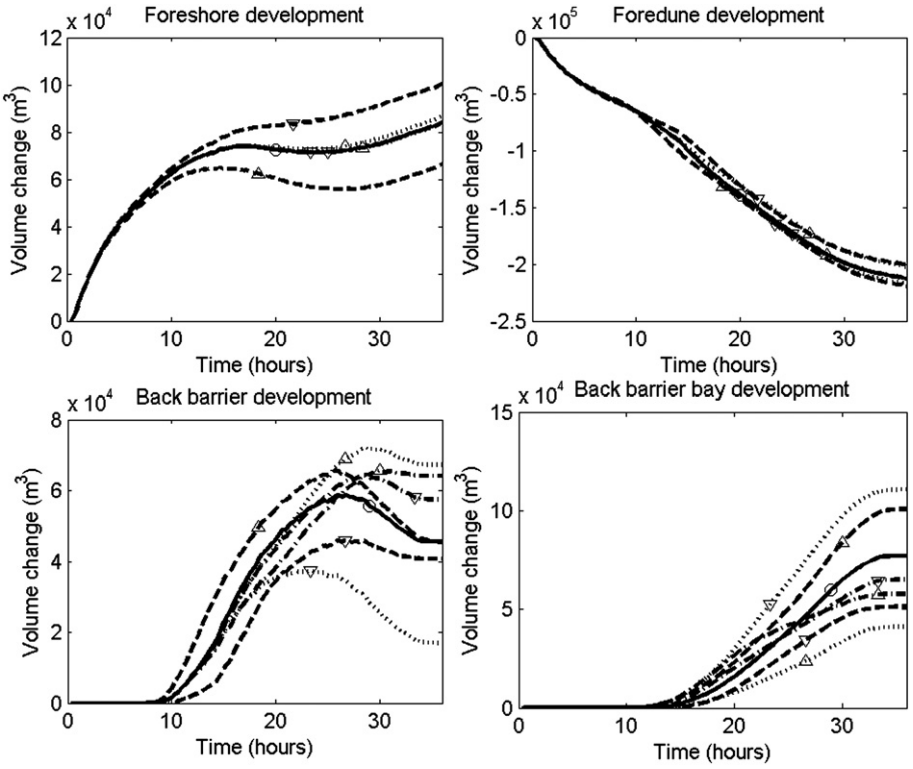

Fig. 14. Morphological development per region for the base simulation (solid line, circle), increased overall surge case (dashed line, up-triangle), decreased overall surge case (dashed line, down-triangle), increased bay surge (dotted line, up-triangle), decreased bay surge (dotted line, down-triangle), 4-hour bay surge delay (dash–dotted line, up-triangle) and 2-hour bay surge delay (dash–dotted line, down-triangle).

The final bed prediction skill is reduced to −2.69, signifying that the prediction is significantly worse than predicting zero bed level change. This suggests that some manner of sediment transport limitation is required in order to simulate high-velocity sediment transport in XBeach. The procedure currently used provides a significant improvement in bed prediction, but can only be regarded as a proxy for an unknown response of the system to the imposed wave and surge conditions. Further investigation of the sediment transport limitation process itself is not possible with the present dataset. However, future overwash modeling would be greatly improved by further research into sediment transport during overwash and the application thereof in numerical models.

7. Conclusions

We have described an application of the XBeach model that solves coupled equations for cross shore and longshore hydrodynamics and morphodynamics in a 2D spatial domain to hurricane conditions. The model was used to simulate the response of a section of Santa Rosa Island, Florida, due to Hurricane Ivan (2004). The predicted topographic response was evaluated against topography collected shortly after hurricane landfall. Measured and modeled wave and surge data were used to generate parametric boundary conditions for the XBeach model. In order to compensate for errors in the best estimate boundary conditions, sensitivity studies were carried out with varying hydraulic forcing, as well as varying model parameters.

The simulation of Santa Rosa Island has shown that XBeach can simulate complex runup and inundation overwash over longshore-varying terrain. The model is capable of producing morphological features common to overwash, such as foredune erosion, back barrier deposition and washover fans. The quantitative skill of the model was determined by comparison with a zero bed level change estimate. Due to lack of post-storm LIDAR data this comparison was limited to the subaerial part of the post-storm barrier island. The model skill was found to be upwards of 0.66 with a mean of 0.72 and the bias was less than −0.21 m with a mean of −0.12 m in simulations in which a sediment concentration limiter was imposed for sheet flow conditions.

The sensitivity simulations in which the hydraulic forcing was varied showed that the skill and bias of the model varied from 0.66 to 0.77 and −0.21 m to −0.04 m respectively, when the forcing was varied within the bounds of this study. This indicates that small differences in the determination of the hydraulic boundary conditions did not lead to significant morphological regime changes on the subaerial part of the barrier island in XBeach and therefore not to significant differences in the model-data comparison. Nonetheless, a qualitative model–model comparison showed interesting responses in the XBeach model to some of the parameter variations in other regions of the barrier island:

- The incident wave height and wave period strongly affect the morphological response of the entire barrier island.
- The start of overwash is determined more strongly by the wave conditions than the overall surge level.
- The overall surge level affects the amount of overwash deposition once overwash has started.
- The surge level gradient across the barrier island affects the back barrier and back barrier bay morphology.

Table 4
Storm duration sensitivity cases.

Duration sensitivity cases			
Name	Change relative to base case	Skill	Bias (m)
Base	–	0.74	−0.13
Longer duration	Entire storm duration increased by 5 h	0.72	−0.16
Shorter duration	Entire storm duration decreased by 5 h	0.75	−0.09

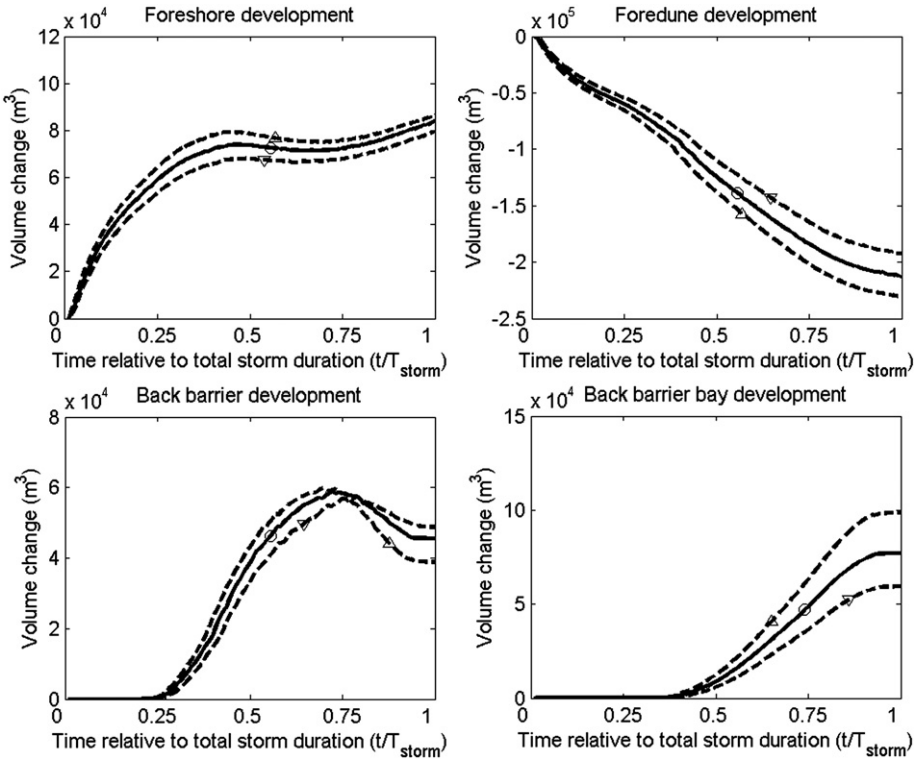

Fig. 15. Morphological development per region for the base simulation (solid line, circle), longer duration case (dashed line, up-triangle) and shorter duration case (dashed line, down-triangle). Note that the horizontal axis has been normalized by the total storm duration.

- A time lag of the surge level in the back barrier bay behind the surge level in the Gulf of Mexico increases the amount of deposition on the back barrier.
- Variations in the storm duration led to different amounts of erosion and deposition on the barrier island and back barrier bay, indicating that the barrier island did not develop an equilibrium profile.

The sensitivity simulations in which the model parameters were varied showed that XBeach is more sensitive to a limiter on sheet flow sediment concentration, than to the variations in hydraulic forcing. It was shown that if no transport limitation is applied, the simulated morphological change on the barrier island is an order of magnitude greater than the measured change. Although the transport limiter parameterization applied on this model improved model results, it can only be considered a proxy for an unknown response of the system to the imposed wave and surge conditions. Further investigation into sediment transport and sediment transport modeling during overwash conditions would greatly improve the reliability of future overwash models.

Table 5
Model parameter sensitivity cases.

Transport limiter sensitivity cases			
Name	Change relative to base case	Skill	Bias (m)
Base	–	0.74	−0.13
Limiter 0.8	Shields value for start of limiter set to 0.8	0.73	−0.05
Limiter 1.2	Shields value for start of limiter set to 1.2	0.68	−0.21
Limiter off	Sediment transport limiter not applied	−2.69	−1.25
Morphological factor 1	Morphological acceleration factor reduced to 1	0.74	−0.13
Morphological factor 5	Morphological acceleration factor reduced to 5	0.73	−0.13

List of symbols

Symbol	Unit	Description
A	J s m^{-2}	Wave action
A_{sb}	s$^{2.4}$ m$^{1.4}$	Bed load coefficient in Soulsby–Van Rijn formulation
A_{ss}	s$^{2.4}$ m$^{1.4}$	Suspended load coefficient in Soulsby–Van Rijn formulation
C	–	Depth-average volumetric sediment concentration
C_d	–	Short wave-related drag coefficient
C_{eq}	–	Depth-average volumetric equilibrium sediment concentration
c_f	–	Coefficient of bed roughness
c_g	m s^{-1}	Wave group velocity
D	W m^{-2}	Wave energy dissipation
D_{50}	m	Median grain diameter
D_s	m^2 s^{-1}	Sediment diffusion coefficient
E	J m^{-2}	Wave or roller energy per unit surface area
F_x	N m^{-2}	x-component of wave and roller forcing
F_y	N m^{-2}	y-component of wave and roller forcing
g	ms^{-2}	Gravitational acceleration, constant 9.81 m s^{-2}
H	m	Wave height
h	m	Water depth
k	m^{-1}	Wave number
p	–	Porosity
S_x	m^2 s^{-1}	x-direction sediment transport rate
S_y	m^2 s^{-1}	y-direction sediment transport rate
$S_{\alpha\beta}$	N m^{-1}	Radiation stress in the direction of the axis α, on the vertical plain normal to the axis β
T	s	Wave period
T_s	s	Sediment adaptation time
t	s	Time
$\|U\|$	m s^{-1}	Absolute total velocity
$\vec{U}$	m s^{-1}	Total velocity vector
u	m s^{-1}	Velocity x-direction
u_{rms}	m s^{-1}	Root-mean-square orbital velocity
v	m s^{-1}	Velocity y-direction
x	m	Horizontal axis coordinate, usually cross shore
y	m	Horizontal axis coordinate, usually longshore
z_b	m	Bed level
Δ	–	Relative density

(continued on next page)

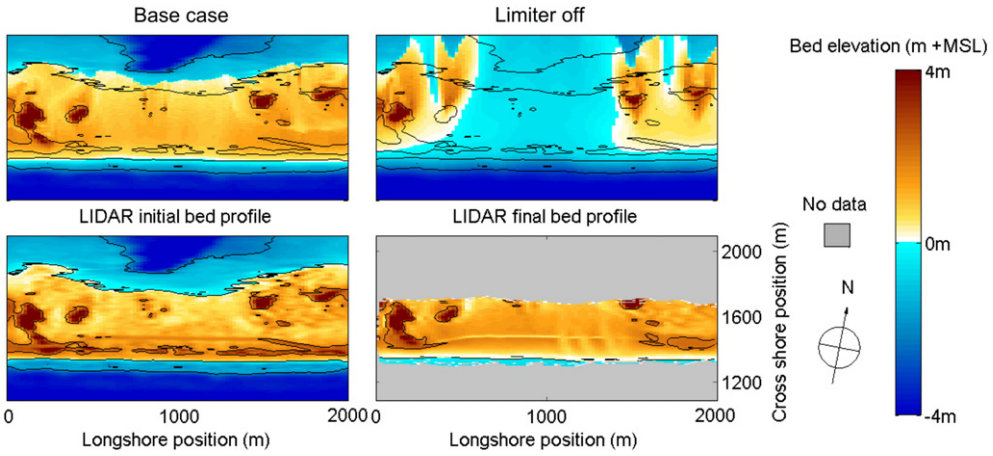

Fig. 16. Final bed elevation in the base case (left panel) and in the case with no sheet flow sediment transport limiter (right panel). Contour lines refer to the initial −2 m, 0 m and +2 m + MSL elevation.

Symbol	Unit	Description
η	m	Water surface elevation
ν_h	$m^2\ s^{-1}$	Horizontal eddy viscosity coefficient
θ	–	Wave angle, the angle between the wave crest normal and the *x*-axis
θ_s	–	Shields parameter
θ_{sf}	–	Shields parameter at which sheet flow occurs
ρ	$kg\ m^{-3}$	Mass density of water
σ	s^{-1}	Intrinsic wave frequency

Acknowledgements

The Research reported in this document has been made possible through the support and sponsorship of the U.S. Government through its European Research Office of the U.S. Army, under Contract no. N62558-06-C-2006, and the Office of Naval Research, in the framework of the NOPP Community Sediment Transport Model project ONR BAA 05-026, through the European Community's Seventh Framework Programme under grant agreement no. 202798 (MICORE Project) and Deltares internal research fund under Strategic Research project 1200266. The USGS Coastal and Marine Geology Program provided support via the National Assessment of Coastal Change Hazards Project and Cooperative Agreement number 06WRAG0045. The help of Dr. Diane Foster in the sheet flow modeling process is much appreciated.

Appendix. List of model parameters

Parameter	Description	Value
alpha	Dissipation parameter in Roelvink (1993) dissipation model	1.0
beta	Slope of breaking wave front in roller model	0.1
C	Chezy roughness value	$55\ m^{1/2}\ s^{-1}$
CFL	CFL number used in computation of automatic timestep	0.8
D50	Median grain diameter	0.0002 m
D90	90-percentile grain diameter	0.0003 m
dico	Horizontal dispersion coefficient	$1.0\ m^2\ s^{-1}$
dryslp	Dry critical bed slope for avalanching	1.0
eps	Cut-off water depth for inundation	0.01 m
facsl	Slope factor in sediment transport formula	1.0
gamma	Breaker parameter in Roelvink (1993) dissipation model	0.55
gammax	Maximum ratio wave height/water depth	5
hmin	Minimum depth for computation of undertow velocity	0.08 m
hswitch	Water depth switch from dry slope to wet slope avalanching	0.1 m
n	Power in breaking probability function	10
nuh	Background horizontal viscosity	$0.01\ m^2\ s^{-1}$
nuhfac	Calibration coefficient in Battjes model of horizontal viscosity	1.0
order	First-order (1) or second-order (2) wave generation	2
por	Porosity	0.4
scheme	First-order upwind (1) or Lax–Wendroff (2) numerical scheme for wave propagation	1
smax	Shields number for start of sheet flow	Varies
Tsfac	Coefficient in adaptation time suspended sediment	0.1
wci	Switch (0/1) to turn on wave-current interaction	0
wetslp	Underwater critical bed slope for avalanching	0.15

References

Andrews, D.G., McIntyre, M.E., 1978. An exact theory of nonlinear waves on a Lagrangian-mean flow. Journal of Fluid Mechanics 89 (4), 609–646.
Bisschop, F., Visser, P., van Rhee, C., 2009. Hindered erosion of granular sediments. Ceda dredging days 2009. Central Dredging Association, Delft.
Booij, N., Ris, R.C., Holthuijsen, L.H., 1999. A third-generation wave model for coastal regions. 1. Model description and validation. Journal of Geophysical Research 104 (C4), 7649–7666.
Bosboom, J., Aarninkhof, S.G.J., Reniers, A.J.H.M., Roelvink, J.A., Walstra, D.J.R., 2000. UNIBEST-TC 2.0 — overview of model formulations. Rep, H2305.42. Delft Hydraulics, Delft.
Brock, J.C., Wright, C.W., Sallenger, A.H., Krabill, W.B., Swift, R.N., 2002. Basis and methods of NASA airborne topographic mapper LIDAR surveys for coastal studies. Journal of Coastal Research 18 (1), 1–13.
Claudino-Sales, V., Wang, P., Horwitz, M.H., 2008. Factors controlling the survival of coastal dunes during multiple hurricane impacts in 2004 and 2005: Santa Rosa barrier island, Florida. Geomorphology 95, 295–315.
Cromwell, J.E., 1971. Barrier coast distribution: a world-wide survey, Second National Coastal and Shallow Water Research Conference. U.S. Office of Naval Research Geography Program. University Press, University of Southern California, Los Angeles, CA, p. 50.
Dean, R.G., 1977. Equilibrium beach profiles: U.S. Atlantic and Gulf coasts. Dept. of Civil Engineering and College of Marine Studies. University of Delaware, Newark.
Deigaard, R., 1993. A note on the three-dimensional shear stress distribution in a surf zone. Coastal Engineering 20, 157–171.
Department of Environmental Protection State of Florida, 2004. Hurricane Ivan Report: Beach and Dune Erosion and Structural Damage Assessment and Post-storm Recovery Plan for the Panhandle Coast of Florida. Tallahassee, Florida.
Divins, D.L. and Metzger, D., 2008. NGDC Coastal Relief Model, http://www.ngdc.noaa.gov/mgg/coastal/coastal.html.
Donnelly, C., Kraus, N.C., Larson, M., 2004. Coastal overwash. Part 1: overview of processes. Regional Sediment Management Demonstration Program Technical Note, ERDC/RSM-TN-14. US Army Engineer Research and Development Center, Vicksburg, Mississippi.
Donnelly, C., Kraus, N., Larson, M., 2006. State of knowledge on measurement and modeling of coastal overwash. Journal of Coastal Research 22 (4), 965–991.
Emanuel, K., Sundararajan, R., Williams, J., 2008. Hurricanes and global warming: results from downscaling IPCC AR4 simulations. Bulletin of the American Meteorological Society 89 (3), 347–367.
Feddersen, F., Guza, R.T., Elgar, S., Herbers, T.H.C., 2000. Velocity moments in alongshore bottom stress parameterizations. Journal of Geophysical Research 105 (C4), 8673–8686.

Fischer, J.S., Overton, M.F., 1984. Numerical model for dune erosion due to wave uprush. 19th Coastal Engineering Conference. ASCE, Houston, pp. 1553–1558.
Galapatti, R., Vreugdenhil, C.B., 1985. A depth-integrated model for suspended sediment transport. Journal of Hydraulic Research 23 (4), 359–377.
Gallagher, E.L., Elgar, S., Guza, R.T., 1998. Observations of sand bar evolution on a natural beach. Journal of Geophysical Research 90, 3203–3215.
Goda, Y., 1985. Random Seas and Design of Maritime Structures. University of Tokyo Press, Tokyo.
Godfrey, P.J., Godfrey, M.M., 1973. Comparison of ecological and geomorphic interactions between altered and unaltered barrier island systems in North Carolina. In: Coates, D.R. (Ed.), Coastal Geomorphology. State Univ. New York, New York, pp. 239–258.
Guza, R.T., Thornton, E.B., 1982. Swash oscillations on a natural beach. Journal of Geophysical Research 87, 483–491.
Hasselmann, K., 1962. On the non-linear energy transfer in a gravity-wave spectrum: I. General theory. Journal of Fluid Mechanics 12, 481–500.
Herbers, T.H.C., Elgar, S., Guza, R.T., 1994. Infragravity–frequency (0.005–0.05 Hz) motions on the shelf. Part I: forced waves. Journal of Physical Oceanography 24 (5), 917–927.
Holthuijsen, L.H., Booij, N., Herbers, T.H.C., 1989. A prediction model for stationary, short-crested waves in shallow water with ambient currents. Coastal Engineering 13, 23–54.
Hosier, P.E., Cleary, W.J., 1977. Cyclic geomorphic patterns of washover on a barrier island in southeastern North Carolina. Environmental Geology 2 (1), 23–31.
Kobayashi, N., Tega, Y., Hancock, M.W., 1996. Wave reflection and overwash of dunes. Journal of Waterway, Port, Coastal and Ocean Engineering 122 (3), 150–153.
Larson, M., Kraus, N., 1989. SBEACH: numerical model for simulating storm-induced beach change. Report 1: Empirical Foundation and Model Development, Technical Report. CERC-89-9. US Army Engineer Waterways Experiment Station, Vicksburg, MS. 267 pp.
Larson, M., Kraus, N., Byrnes, M.R., 1990. SBEACH: numerical model for simulating storm-induced beach change. Report 2: Numerical Formulation and Model Tests, Technical Report. CERC-89-9. US Army Engineer Waterways Experiment Station, Vicksburg, MS. 120 pp.
Larson, M., Wise, R.A., Kraus, N., 2004. Modelling dune response by overwash transport. In: Mckee Smith, J. (Ed.), Coastal Engineering 29th International Conference. World Scientific, Lisabon, Portugal, pp. 2133–2145.
McCall, R.T., 2008. The longshore dimension in dune overwash modelling. Development, Verification and Validation of XBeach. Delft University of Technology, Delft.
Morton, R.A., Sallenger, A.H., 2003. Morphological impacts of extreme storms on sandy beaches and barriers. Journal of Coastal Research 19 (3), 560–573.
National Hurricane Center, 2008. Tropical Cyclone Report. In: Stewart, S.R. (Ed.), Hurricane Ivan. http://www.nhc.noaa.gov/.
Plant, N.G., Holland, K.T., Puleo, J.A., 2002. Analysis of the scale of errors in nearshore bathymetric data. Marine Geology 191, 71–86.
Raubenheimer, B., Guza, R.T., 1996. Observations and predictions of run-up. Journal of Geophysical Research 101 (C10), 25575–25587.
Reniers, A.J.H.M., 1999. Longshore Current Dynamics. Delft University of Technology, Delft.
Reniers, A.J.H.M., Roelvink, J.A., Thornton, E.B., 2004. Morphodynamic modeling of an embayed beach under wave group forcing. Journal of Geophysical Research 109 (C01030).
Roelvink, J.A., 1993. Dissipation in random wave groups incident on a beach. Coastal Engineering 19, 127–150.
Roelvink, J.A., Stive, M.J.F., 1989. Bar-generating cross-shore flow mechanisms on a beach. Journal of Geophysical Research 94 (C4), 4785–4800.
Svendsen, I.A., 1984. Wave heights and set-up in a surf zone. Coastal Engineering 8, 303–329.
Roelvink, J.A., et al., 2008. Modeling Hurricane Impacts on Beaches, Dunes and Barrier Islands, ICCE 2008. Hamburg.
Roelvink, J.A., et al., 2009. Modeling storm impacts on beaches, dunes and barrier islands. Coastal Engineering 56, 1133–1152.
Sallenger, A.H., 2000. Storm impact scale for barrier islands. Journal of Coastal Research 16 (3), 890–895.
Soulsby, R., 1997. Dynamics of Marine Sands. Thomas Telford Publications, London.
Stelling, G.S., Duinmeijer, S.P.A., 2003. A staggered conservative scheme for every Froude number in rapidly varied shallow water flows. International Journal for Numerical Methods in Fluids 43 (12), 1329–1354.
Stive, M.J.F., Wind, H.G., 1986. Cross-shore mean flow in the surfzone. Coastal Engineering 10, 325–340.
Suter, J.R., Nummedal, D., Maynard, A.K., Kemp, P., 1982. A process–response model for hurricane washovers. 18th Coastal Engineering Conference, Capetown, pp. 1459–1789.
Svendsen, I.A., Haas, K., Zhao, H., 2002. Quasi-3D Nearshore Circulation Model SHORECIRC. University of Delaware, Newark.
Tuan, T.Q., Verhagen, H.J., Visser, P., Stive, M.J.F., 2006. Numerical Modelling of Wave Overwash on Low-crested Sand Barriers, 30th Coastal Engineering Conference. World Scientific, San Diego.
van Dongeren, A.R., Svendsen, I.A., 1997. Absorbing-generating boundary condition for shallow water models. Journal of Waterway, Port, Coastal and Ocean Engineering 123 (6), 303–313.
van Dongeren, A.R., Sancho, F.E., Svendsen, I.A., Putrevu, U., 1994. SHORECIRC: a quasi 3-D nearshore model. 24th International Conference on Coastal Engineering. Am. Soc. of Civ. Eng., Kobe, pp. 2741–2754.
van Dongeren, A.R., Reniers, A.J.H.M., Battjes, J.A., 2003. Numerical modeling of infragravity waves response during DELILAH. Journal of Geophysical Research 108 (C9), 3288.
van Gent, M.R.A., van Thiel de Vries, J.S.M., Coeveld, E.M., De Vroeg, J.H., van de Graaff, J., 2008. Large-scale dune erosion tests to study the influence of wave periods. Coastal Engineering 55, 1041–1051.
van Rhee, C., 2007. Erosion of granular sediments at high flow velocity, Hydrotransport 17. The 17th International Conference on the Hydraulic Transport of Solids. BHR Group, Cape Town, South Africa.
van Rhee, C., Talmon, A.M., 2000. Entrainment of sediment (or reduction of sedimentation) at high concentration. Proc. 10th International Conference on Transport, and Sedimentation of Solid Particles, Wroclaw, Poland.
van Rijn, L.C., 1993. Principles of Sediment Transport in Rivers, Estuaries and Coastal Seas. Part I: Edition 1993. Aqua Publications, Amsterdam.
van Thiel de Vries, J.S.M., 2009. Dune erosion during storm surges. PhD Thesis, Delft University of Technology, Delft.
van Thiel de Vries, J.S.M., van Gent, M.R.A., Walstra, D.J.R. and Reniers, A.J.H.M., 2008. Analysis of dune erosion in large scale flume experiments. Coastal Engineering, Awaiting publication.
Vellinga, P., 1986. Beach and Dune Erosion during Storm Surges, PhD thesis, Delft University of Technology, Delft.
Wang, R., Manausa, M., 2005. Hurricane Ivan: Characteristics and Storm Tide Evaluation. Florida Department of Environmental Protection, Tallahassee, Florida.
Wang, P., et al., 2006. Morphological and sedimentological impacts of Hurricane Ivan and immediate poststorm beach recovery along the northwestern Florida Barrier-Island Coasts. Journal of Coastal Research 22 (6), 1382–1402.
Winterwerp, J.C., 2001. Stratification effects by cohesive and noncohesive sediment. Journal of Geophysical Research 106 (C10), 22,559–22,574.